Cellular response to heat shock studied by multiconfocal Fluorescence Correlation Spectroscopy

Meike Kloster-Landsberg,[†] Gaëtan Herbomel,[‡] Irène Wang,[†] Jacques Derouard,[†] Claire Vourc'h,[‡] Yves Usson,[§] Catherine Souchier,[‡] and Antoine Delon[†*]

[†]Univ. Grenoble 1 / CNRS, LIPhy UMR 5588, Grenoble, F-38041, France
[‡]Univ. Grenoble 1 / INSERM, IAB CRI U823 team 10, Grenoble, F-38042, France
[§]Univ. Grenoble I / CNRS, TIMC-IMAG UMR5525, Grenoble, F-38706, France

---

SUPPORTING MATERIAL: Methods and complementary results

S1 MULTICONFOCAL FCS SET-UP

Our home-built mFCS set-up (see Fig. S1) is based on an inverted microscope stand (Olympus IX70, Olympus, Hamburg, Germany). The FCS excitation source is a solid-state laser emitting up to 20mW of 488 nm-wavelength continuous-wave light (85-BCD-020, CVI Melles Griot, Albuquerque, NM). The beam is sent into a single-mode fiber in order to spatially clean its wavefront. Then it can be directed to two different optical paths: one direct path (not shown) where the beam is simply expanded by a telescope before reaching the microscope objective and a second path where a Spatial Light Modulator (SLM) composed of 800×600, 20 μm-pixels (LCOS-SLM X10468-01, Hamamatsu, Massy, France) is used for wavefront shaping. Before reaching the SLM, the beam is expanded using a telescope to cover the active area of the SLM, and goes through a half-wave plate and a polarizer (not shown) since the SLM only diffracts horizontally polarized radiation. When the adequate phase map is addressed to the SLM, the beam is focused in a plane which is optically conjugated with the microscope object plane. The beam is then collimated before being reflected by a dichroic mirror (PB 505, Olympus) towards a water immersion objective lens (Plan-apo 60×, NA=1.2, Olympus, France). This collimating lens is also used to image the SLM onto the back focal aperture of the objective lens to ensure that all the diffracted light is coupled into the objective. When one spot is created with the SLM, the laser power within the sample is measured to be about 6 times lower than the laser power at the exit of the single-mode fiber. When five spots are created, the total power into the spots is about 30% lower, due to non-diffracted light (zeroth order) reflected by the SLM. All the values given below refer to the power measured at the exit of the single-mode fiber. For the wide-field fluorescence imaging, we have added a custom-built illumination device based on a Light-Emitting Diode (LED) (Philips, Luxeon Rebel LXML-PB01-0023) with a center emission wavelength of 470 nm. This excitation light is coupled into the microscope by a dichroic mirror (Semrock, LaserMUX LM01-480-25), which transmits the laser beam and reflect the LED light, so that both excitation sources can be sent on the sample.

Fluorescence emitted by the sample is spectrally filtered (PH 510, Olympus) (not shown) then sent to a side port of the microscope where it can be directed either to a CCD camera for imaging (Clara, Andor Technology, Belfast, Northern Ireland) or to one of the two detection paths for FCS measurements. The first leads to a multimode fiber of 100 μm core diameter

connected to an Avalanche PhotoDiode (APD) (SPCM-AQR-13, Perkin Elmer, Waltham, MA) for standard FCS measurements. The fiber core acts as a pinhole to ensure confocal detection. The magnification in this path is 5.3× (resulting in a total magnification 316× from the microscope object plane). The second path leads to an EMCCD camera with 128×128 pixels of 24 µm (iXon+ DU860, Andor Technology, Belfast, Northern Ireland) for the parallel multi-spot FCS measurements. In this path, a mask (consisting of a razor edge) is positioned in a plane conjugated to the microscope object plane to prevent the out-of-focus light from illuminating unused parts of the EMCCD chip. Then a pair of achromatic lenses demagnifies the fluorescence image before it is sent to the EMCCD. In this case, each pixel of the camera acts as an individual pinhole for parallel confocal detection. The magnification of 1.3× in this path (resulting in a total magnification of 79×) has been adjusted so that the EMCCD 24 µm-pixels result in collection volumes of approximately the same size as the 100µm-fiber core in the first path.

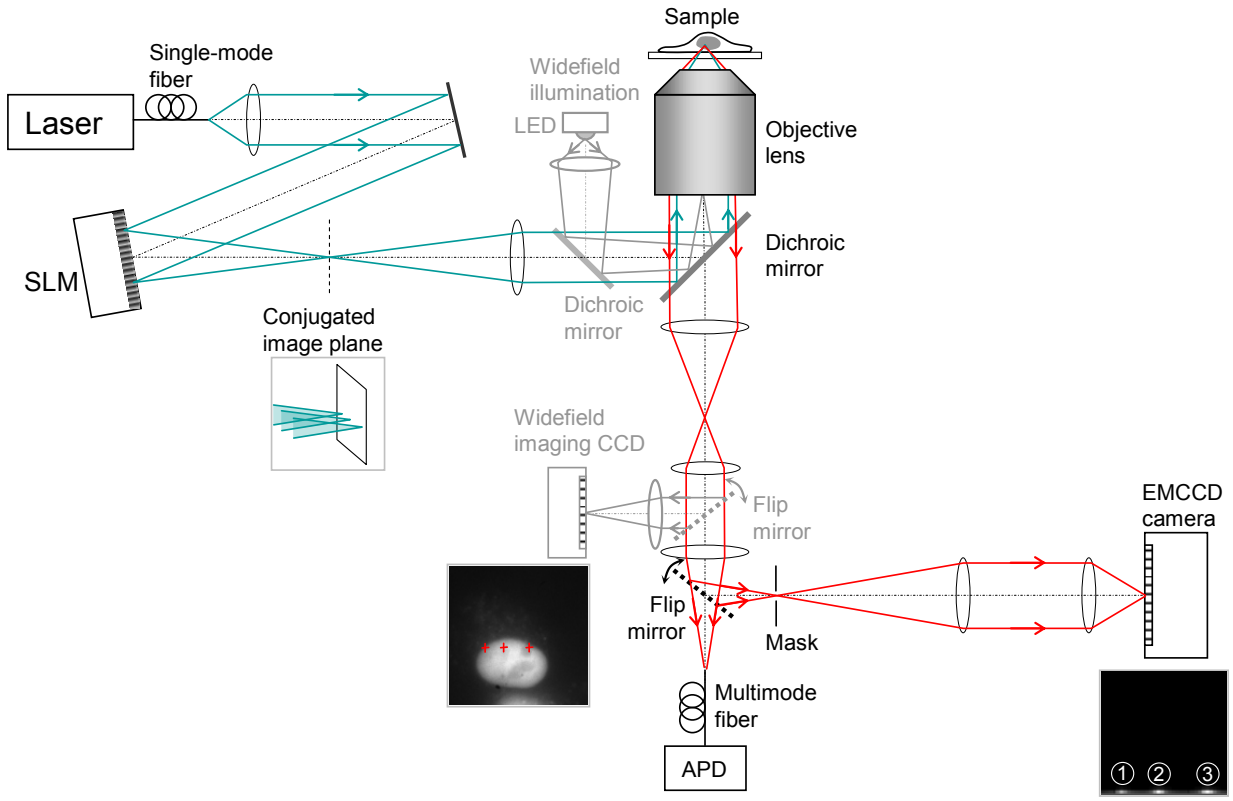

Figure S1: Experimental setup used for multiconfocal FCS measurements: the SLM creates several spots which are imaged on the bottom row of the EMCCD chip. The elements used for widefield fluorescence microscopy are depicted in gray.

S2 SLM PHASE MAP CALCULATION

In our case, all the spots are created in the same plane on the z-axis, optically conjugate with the microscope object plane. This plane, which can be considered as the SLM focal plane, is

at a distance f (we used f = 364 mm throughout this work) from the SLM. It should be noted that off-focus spots could be obtained exactly in the same way, if this focal distance is made to vary. It is also worthwhile to stress the fact that the SLM cannot create the exact field since it can only modulate the phase of the incident wave and not its intensity.

If $r_m(x,y)$ is the distance between the pixel of the SLM at coordinates x,y and the m^{th} spot, the phase pattern applied to the SLM is given by:

$$\phi(x,y) = \arg\left(\sum_m a_m \frac{\exp\left[-i \frac{2\pi}{\lambda} r_m(x,y) + \theta_m \right]}{r_m(x,y)} \right) \tag{S2}$$

where a_m is an amplitude factor that takes into account the obliquity factor, and θ_m are random phases (uniformly distributed in $[0,2\pi]$). This expression represents the phase of a superposition of several spherical waves converging at the desired spots. Random phases were added to each spot in order to minimize interference effects leading to the occurrence of ghost spots. The presence of ghost spots in itself is not a problem for mFCS, since only the signal of relevant pixels of the camera is taken into account. However, they deviate part of the available laser energy from useful spots and may also damage the sample. The introduction of random phases effectively reduces the intensity of ghost spots.

This 'spherical random superposition' algorithm saves a lot of computational time. Diffraction-limited spots can be generated with reasonably good efficiency. However, they are not perfectly uniform in intensity: we observe a typical intensity variation of 20% between the spots. It is shown in the Results section that FCS measurements are not affected by this non-uniform distribution, provided the data are corrected for signal crosstalk between adjacent spots.

For mFCS experiments with the EMCCD camera, it is important that each spot is centered on one pixel of the EMCCD to ensure a correct shape of the detection volume. Therefore, we developed an automatic procedure to find the optimum coordinates for each spot. First, the center of each spot is determined with sub-pixel accuracy by three-point Gaussian fits and brought in reasonable coincidence with the pixel center. Then, we apply an iterative procedure to adjust the spot position more precisely.

S3 DATA ACQUISITION AND PROCESSING

To perform the mFCS data acquisition and processing we developed an interface in MATLAB (MathWorks, Natick, MA), which allowed us to control the SLM and the EMCCD camera for multi-spot generation and detection, in addition to the microscope stage and a CCD camera for imaging and selecting the cells. The Andor Software Development Kit was used to access the two cameras via MATLAB. The EMCCD camera was operated in a frame transfer mode with the electron multiplying gain set to 300 and a vertical shift speed to 0.25µs. In order to attain a sufficient time resolution, we used the Crop FvB (Full vertical Binning) readout mode throughout the present work. Since, in this mode, charges coming from the same column are binned vertically before the read out, the unused parts of the chip have to be blinded in order to prevent out of focus light from deteriorating the signal. The fluorescence signal was focused on

pixels in the bottom row of the camera chip while a razor edge masked the upper part. Thus a frame rate of 70 kHz could be achieved, the price to pay being that all the spots had to be aligned on a single row. Each acquisition consisted of a 10s recording (a kinetics series of 700000 images), that was spooled to a hard drive in order to be able to continue directly with the next acquisition. After a series of five acquisitions, an offset measurement was recorded with the laser off. Among the 128 pixels of the last row, the first five pixels were always masked and their mean value was used to subtract the electronic offset to each acquisition, since its level varies from one acquisition to another.

The signal from each bright pixel was extracted as a function of time. The level of the corresponding pixels in the adjusted offset acquisition was also extracted. Both the offset and the signal level generally exhibited a drift during the acquisition. To extract this drift, a polynomial fit to the 6^{th} order was applied to the time traces. The smoothed offset trace, given by the polynomial fit, was subtracted to the acquired signal trace. Then the resulting trace was divided by the polynomial fit of the signal, in order to remove drifts that could be generated by the electronics, photobleaching effects or slight cell motility and deformation. This corrected time trace was used to calculate the ACF with MATLAB. The time interval between data points in the ACF curve increases almost exponentially with increasing delays. All the ACF curves presented here have been averaged over at least 5 acquisitions, thus providing a mean and a Standard Error (SE) of the mean for each data point to perform weighted fits of the ACF.

In addition to the ACF our software calculates, for each spot, the intensity at the beginning of the acquisition, which can be divided by the number of molecules to provide the molecular brightness (by analogy with the APD acquisitions).

S4 PERFORMANCES OF EMCCD VERSUS APD DETECTION FOR FCS

APDs are the most common detectors for FCS. They detect single photons with the advantage of high quantum efficiency, low dark counts and good temporal resolution. For multiple spot parallel measurements, we have chosen an EMCCD camera, because it is capable of detecting single photons thanks to the electron multiplication process. However, EMCCDs are intrinsically noisier than APDs. The dominant sources of noise are the so-called Clock Induced Charge due to charge transfer (in our case, it is a background of approximately 3500 events/sec) and the fluctuations of the electronic offset and of the multiplication gain. Therefore, it is important to experimentally investigate how these factors impact FCS measurements.

To assess the relative performances of APD and EMCCD as detectors for FCS, we performed a number of measurements by varying both the excitation power and the concentration of Dextran-Rhodamine Green in aqueous solution as shown on Fig. S4. Five spots in a row were created by the SLM and the fluorescence signal from the central spot was detected either by the APD or the EMCCD camera. When the resulting ACF exhibits sufficient signal to noise ratio to yield reliable estimations of the fit parameters N and τ_D, the data were considered as usable.

In order to compare the performances of the two detectors directly, all resulting ACFs have been fitted with a simple model without taking into account the artefactual oscillation appearing at long lag times (> 1 s) for measurements on the EMCCD camera. Furthermore, only the offset has been subtracted to the EMCCD signal without performing a correction for cross-talk and background caused by adjacent spots.

Hatched areas in Fig. S4 depict the appropriate measurement conditions for each detector. We note that the EMCCD camera is not suitable for measurements with a low total count rate (either low excitation power or low concentration), which is expected since the fluorescence signal would need to dominate the detector noise. However, the EMCCD performance comes close to that of the APD.

Please note that the fit to the data measured by the EMCCD camera can be improved by taking into account the artifactual oscillation in the ACFs that gets particularily disturbing for low count rates. Moreover, some experimental conditions are in favor of EMCCDs. This is the case for strong fluorescence signals presenting a risk of saturation and damage to the APD, while the EMCCD can still be used, as shown for the upper-right corner of the graph. Although it was not necessary in our case, the EMCCD saturation level could be further pushed up by adjusting the multiplication gain, which proves advantageous when studying particles with high brightness or high concentrations.

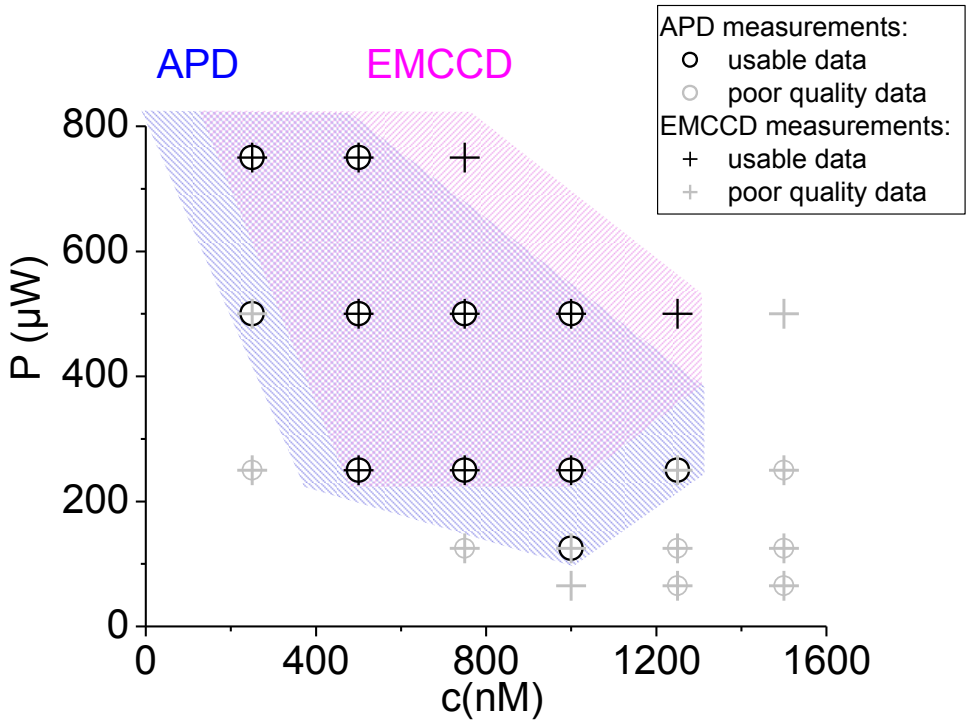

Figure S4 : Performance of the EMCCD camera (crosses) as a detector for mFCS compared to the standard avalanche photodiode (circles). Measurements have been performed with five spots created by the SLM and by varying both the excitation power and the fluorophore concentration. If the signal to noise ratio is large enough to allow a confident fit of the ACF, black symbols are used. Otherwise, gray symbols are drawn. The hatched areas illustrate the regions where the APD (*blue descending lines*) or EMCCD (*magenta ascending lines*) are usable.

S5 FCS CALIBRATION MEASUREMENTS IN SOLUTION

To characterize our experimental system under controlled conditions, we have performed FCS measurements in solution. First, single spot measurements are presented in order to calibrate

the observation volume of our multiconfocal FCS setup. The EMCCD detection path has been characterized relative to the APD path. We have verified that the experiment provides reliable results on a wide range of concentrations. Then, the consequence of moving the excitation spot away from the optical axis is investigated. For single spot, the laser power at the exit of the single-mode fiber was set to 80 µW. Finally, how the generation of multiple excitation spots would affect the effective volume and FCS results is examined.

Calibration with APD detection

The reference solution chosen for FCS measurements with the EMCCD camera is Dextran-Rhodamine Green 10 kDa in water, because this molecule has a large size and consequently a low diffusion constant, which ensures that its residence time in the observation volume is compatible with the time resolution of the EMCCD camera (limited to 14 µs). In order to determine the diffusion coefficient of this compound, we have measured its residence time as well as that of Rhodamine 6G in the exactly same conditions. Thus, using the SLM to generate a single spot and the APD for detection, we obtained at 37°C, τ_D = 20 µs for Rhodamine 6G and τ_D = 69 µs for Dextran-Rhodamine Green 10kDa. We use as reference the previously published value of Rhodamine 6G diffusion coefficient determined by 2 foci FCS (1). After correcting for the change of water viscosity with temperature, the reference value for Rhodamine 6G at 37°C is D_{R6G} = 555 µm^2/s. The corresponding lateral width of the observation volume is w_r = 0.211 µm for the present configuration (SLM and APD). Then, we deduce the diffusion coefficient of Dextran-Rhodamine Green at 37°C D_{Dext} = 161 µm^2/s.

FCS measurements as a function of fluorophore concentration

To ensure that a wide range of concentrations could be reliably measured, FCS measurements in Dextran-Rhodamine Green solutions of increasing concentrations were performed using a single SLM generated spot and both detection pathways, one leading to the APD and the other to the EMCCD. The ACF curves were fitted to yield the average number of molecules and the diffusion times. The resulting diffusion times remain constant throughout the concentration range (the values measured with the EMCCD are larger by a factor 1.4 than those obtained with the APD). The average number of molecules varies linearly with the concentration over the entire span of concentrations (200 nM to 1200 nM), as shown in Fig. S5-1. A steeper slope is observed for the data obtained with EMCCD detection which reveals an enlarged observation volume. From the slopes, we estimate the increase in effective volume to be 30% for EMCCD compared to APD. Taking into account the optical magnification, one EMCCD pixel corresponds to a 96µm square in the plane of the 100µm-diameter optical fiber coupled to the APD, so that the EMCCD detector area is larger by 17%. A possible axial elongation can also contribute to the volume enlargement, although the *S* factor, which is related to this elongation, was estimated to be about 5, both for APD and EMCCD detection. The *S* value was thus set to 5 throughout this study. Other factors may contribute to the volume enlargement such as defocus or aberrations introduced by the additional pair of lenses on the EMCCD path. One also observes in Fig. S5-1 that the extrapolation of the EMCCD data points at null concentration would not lead to a null number of molecules. We interpret this as a consequence of a remaining, uncorrelated, signal background from the EMCCD. As a matter of fact, it is known that a background would cause an artificially increased number of molecules that is not proportional to the actual number of molecules.

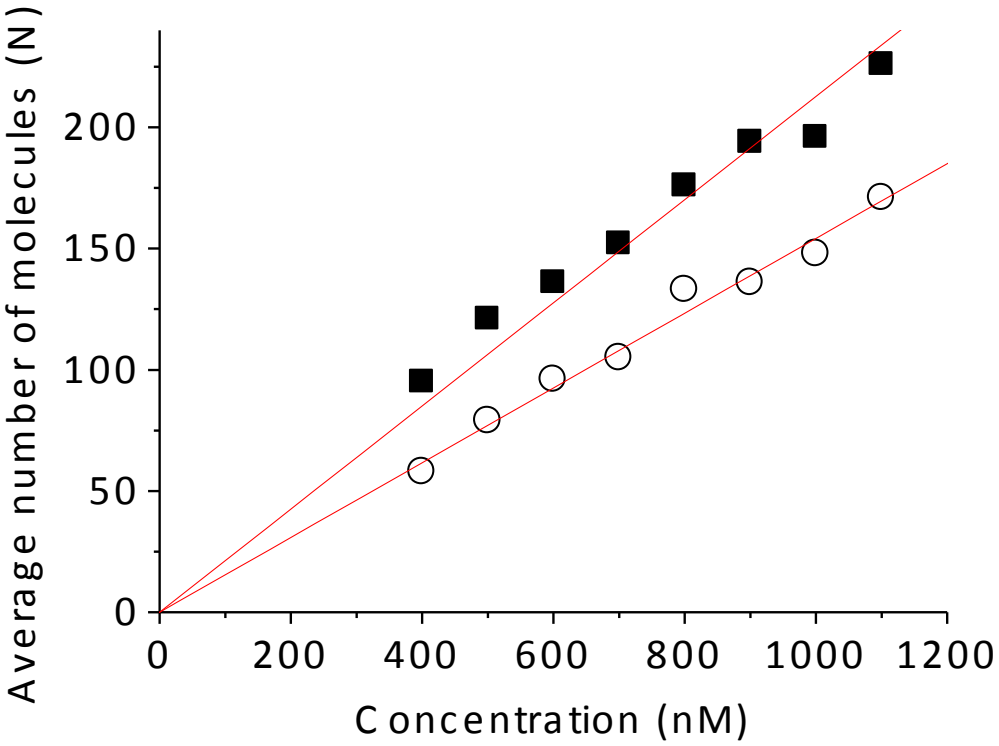

Figure S5-1: Average number of molecules in solutions of Dextran-Rhodamine Green estimated from FCS measurements as a function of the concentration, for APD (*open circles*) and EMCCD (*solid squares*) detection. Data are fitted with a linear function (*solid red line*).

Finally, using the ratio between the diffusion times measured using the EMCCD *versus* the APD and the previous calibration of the APD detection path, the lateral dimension of the observation volume (assumed 3D Gaussian) is found to be $w_r = 0.251$ µm, for the overall setup which combines the SLM (to generate a single spot) and the EMCCD.

Off-axis single spot measurements

To assess the performances of our system for off-axis measurements, we used the SLM to create single excitation spots at various distances from the center of the field. The measured ACF curves are fitted to yield N and τ_D which are depicted as a function of distance to the optical axis in Fig. S5-2. We can observe a general trend for N and τ_D to increase when the spot is moved away from the center, which is expected since the optical aberrations are larger when the objective is used off-axis. Throughout the region imaged on the EMCCD camera which corresponds to a 38 µm square in object space, N and τ_D vary by less than 20 %. For our measurements in cells, all spots are within a 10 µm wide region. Therefore, we have ignored the off-axis deviation which is negligible compared to other sources of variations.

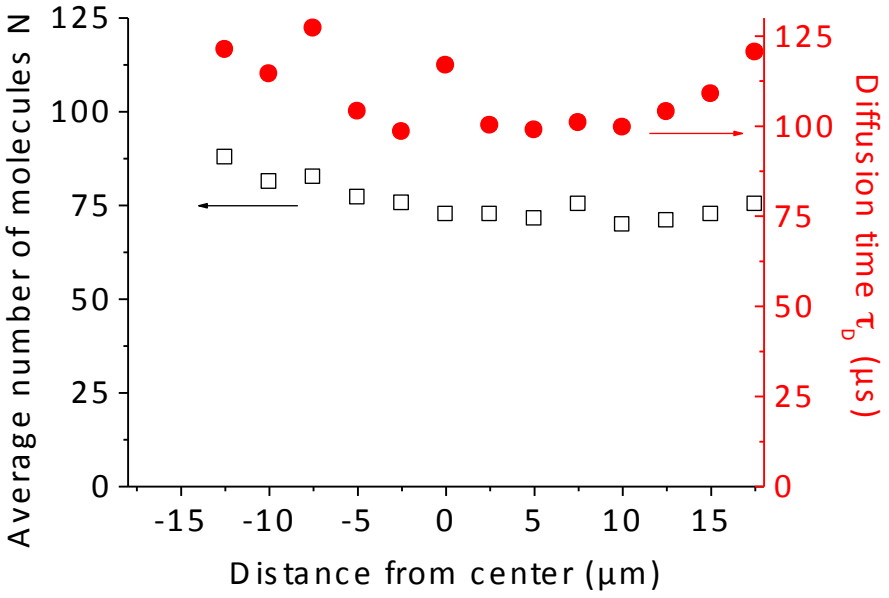

Figure S5-2: Off-axis FCS measurements in an aqueous solution of Dextran-Rhodamine. The SLM was used to generate a spot at different distances from the microscope optical axis. Fluorescence was detected with the EMCCD camera. The fit of the ACF curves yielded values of the number of molecules (*open squares*) and the diffusion time (*solid circles*) shown as a function of the distance to the optical axis.

Multiple spot generation

Up to now, the SLM has been used to generate only one spot. To determine whether the confocal volume would change when several excitation spots are simultaneous generated, the SLM was used to create five spots in a row in a solution. Only the signal from the center spot was extracted and the corresponding ACF is compared to those obtained with a single excitation spot. We could conclude that no widening of the effective volume is observed since the diffusion time is unchanged compared to the single spot case. However, a problem of fluorescence background occurs in the case of multiple spots generation, which will be dealt in the next paragraph.

S6 CORRECTION OF CROSS-TALK IN MULTISPOT MEASUREMENTS

When several excitation spots are created in close vicinity as required for multispot FCS, some cross-talk may occur between adjacent spots. Indeed, when the excitation beam is focused into a homogeneous solution, the fluorescence image displays a central peak with a halo that extends to some distance. Therefore, when several spots are generated, the signal received on an EMCCD pixel centered on one spot includes contributions from the side wings of adjacent spots. These contributions can be considered as an unwanted background and result in an artificial increase of the estimated number of molecules compared to the single spot case. Since the amount of cross-talk depends on the distance between spots and the relative intensity of the spots, the estimated number of molecules would also depend on these factors and vary from spot to spot. This problem is even more serious considering the fact that, as mentioned previously, it is

difficult to control the relative intensity between the spots when calculating the SLM phase map. As shown in the averaged profile of Fig. S6 *A*, the spot intensities can differ by as much as 40 %. In order to solve this problem, we used the following method: first, the intensity profile averaged over the first 10000 frames of each measurement was calculated (after the electronic offset removal) and fitted to a multipeak Lorentzian function, as depicted in Fig. S6 *A*. The Lorentzian peak is a reasonable approximation of the fluorescence profile in the vicinity of a spot, although it does not perfectly describe the shape of the low intensity wings. To obtain a good quality fit, it was necessary to add a constant offset to the five Lorentzian peaks. This offset accounts for both the non-perfect fit of the peaks by Lorentz functions and unfocused background due to non-diffracted light (zeroth order) reflected by the SLM. For each spot, the background level, which includes contributions from the other peaks and the global offset, is subtracted from the recorded fluorescence time trace before calculating the ACF. Fig. S6 *B* shows the resulting ACF curves of the 5 spots after this correction. One can see that they are very similar despite the variability of the spot intensities. Moreover, the fits of these ACF curves yielded estimated numbers of molecules and diffusion times that are fairly consistent and that clearly do not depend on the intensity of each spot (see Fig. S6 *B* inset).

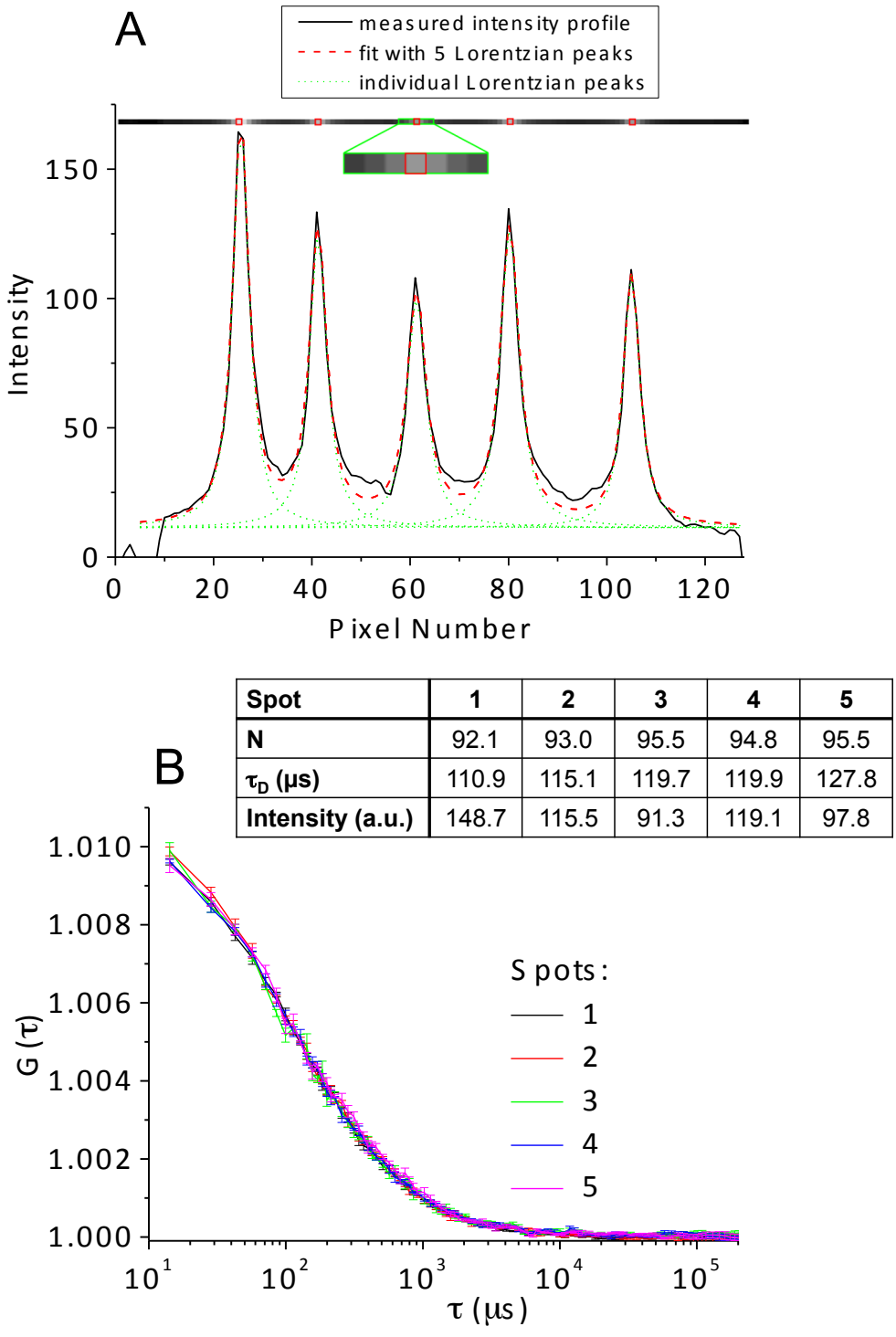

Spot	1	2	3	4	5
N	92.1	93.0	95.5	94.8	95.5
τ_D (μs)	110.9	115.1	119.7	119.9	127.8
Intensity (a.u.)	148.7	115.5	91.3	119.1	97.8

Figure S6: Correction for cross-talk between adjacent spots in Dextran-Rhodamine Green solution for simultaneous ACF measurements over 5 spots. (*A*) Intensity profile measured by the EMCCD averaged over 10000 frames (*solid black line*) fitted using a multi-peak Lorentzian function (*dashed red line*) which is the sum of individual Lorentzian peaks and a global offset (*dotted green lines*). The image of the bottom row of the EMCCD chip is also shown as inset, where the 5 individual pixels (among 128) used as individual pinholes, to

calculate the ACF, are surrounded with red squares. (*B*) ACF curves calculated from the signal of each spot after removing the background and the contributions from other spots. Note that the autocorrelation curves are indistinguishable. The resulting fit parameters (number of molecules and diffusion times) and the corrected spot intensities are shown in the inset.

S7 DIFFUSION COEFFICIENT OF EGFP IN SOLUTION

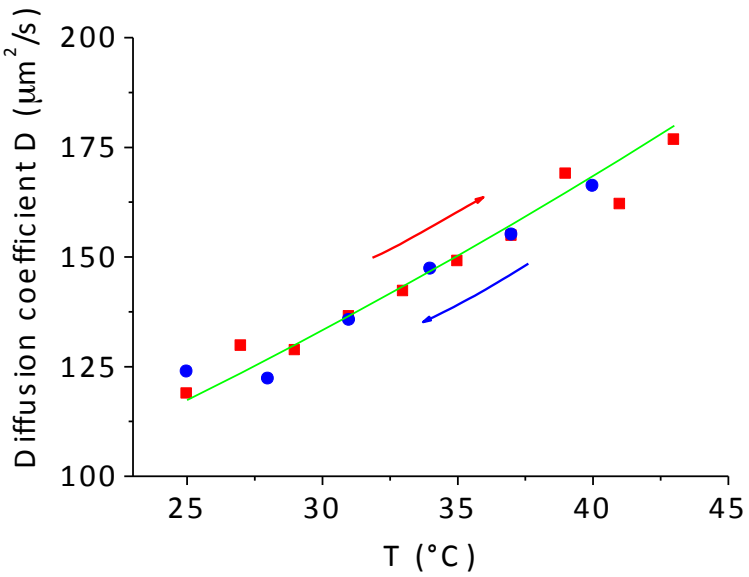

Figure S7: Diffusion coefficient of eGFP in aqueous solution measured as a function of temperature during heating (*red solid squares*) and cooling (*blue solid circles*). The expected temperature dependence when taking into account water viscosity changes is also depicted (*green solid line*).

S8 DISTRIBUTIONS OF THE DYNAMIC CONSTANTS

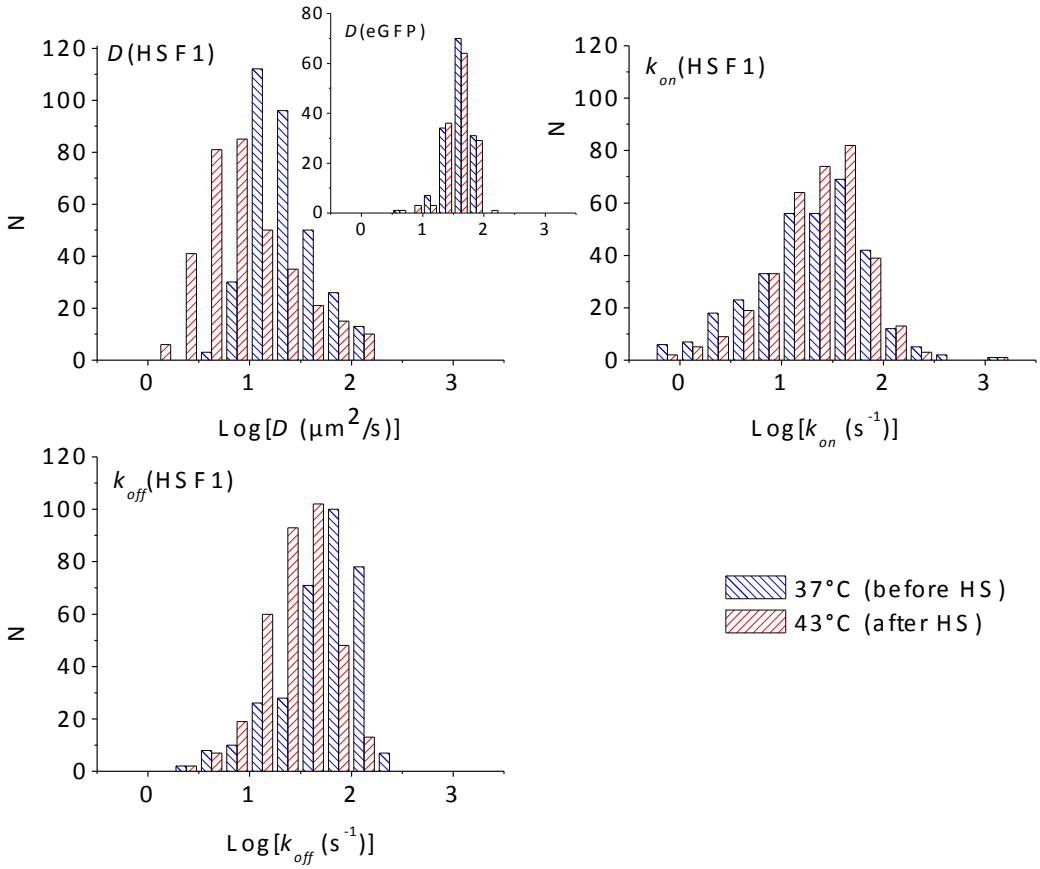

Figure S8: Histograms of the logarithm of the dynamic constants, D, k_{on} and k_{off} for HSF1-eGFP cells, before (descending blue patterns) and after heat shock (ascending red patterns), calculated from the fitted parameters of 674 ACF curves. Clearly, at 43°C, the distribution of the HSF1 diffusion constant, D, extends to lower values and widens, while that of k_{on} is almost unchanged and that of k_{off} shifts to lower values. The inset in the histogram of the HSF1 diffusion constant shows, for comparison, the narrower, temperature independent, histogram of the diffusion constant of inert eGFP molecules.

SUPPORTING REFERENCES

(1) Müller, C. B., A. Loman, V. Pacheco, F. Koberling, D. Willbold, W. Richtering, and J. Enderlein. 2008. Precise measurement of diffusion by multi-color dual-focus fluorescence correlation spectroscopy. *Europhys. Lett.* 83:46001-p1-46001-p5